Kinetic model of primary energy transfer and trapping in photosynthetic membranes

Tõnu Pullerits and Arvi Freiberg
Institute of Physics, Estonian Academy of Sciences, 202400 Tartu, Estonia

ABSTRACT The picosecond time-domain incoherent singlet excitation transfer and trapping kinetics in core antenna of photosynthetic bacteria are studied in case of low excitation intensities by numerical integration of the appropriate master equation in a wide temperature range of 4–300 K. The essential features of our two-dimensional-lattice model are as follows: Förster excitation transfer theory, spectral heterogeneity of both the light-harvesting antenna and the reaction center, treatment of temperature effects through temperature dependence of spectral bands, inclusion of inner structure of the trap, and transition dipole moment orientation. The fluorescence kinetics is analyzed in terms of distributions of various kinetic components, and the influence of different inhomogeneities (orientational, spectral) is studied.

A reasonably good agreement between theoretical and experimental fluorescence decay kinetics for purple photosynthetic bacterium *Rhodospirillum rubrum* is achieved at high temperatures by assuming relatively large antenna spectral inhomogeneity: 20 nm at the whole bandwidth of 40 nm. The mean residence time in the antenna lattice site (it is assumed to be the aggregate of four bacteriochlorophyll *a* molecules bound to proteins) is estimated to be ~12 ps. At 4 K only qualitative agreement between model and experiment is gained. The failure of quantitative fitting is perhaps due to the lack of knowledge about the real structure of antenna or local heating and cooling effects not taken into account.

I. INTRODUCTION

Pigments and protein polypeptides in photosynthetic membranes are noncovalently bound and form functionally defined large macromolecules, pigment-protein complexes (1). Two main types of pigment-protein complexes are of interest here: the so-called light-harvesting antenna pigment-protein complexes (LHC) and the reaction center (RC) pigment-protein complexes. LHCs function to absorb light energy and to transfer it in the form of incoherent singlet electronic excitations of pigments (2, 3) with minimal losses (that means very fast) to RCs, where within several picoseconds the separation of charges takes place. Thus, potential energy is conserved to drive various biochemical reactions in photosynthetic organisms (4).

First, pigment content, and thereafter the pigment-pigment and pigment-protein interactions, determines the spectral properties of LHCs and of RCs. For example, one of the simplest photosynthetic organisms, a bacteriochlorophyll (BChl) *a* containing purple bacterium *Rhodospirillum (R.)* rubrum, is characterized with a single broad absorption band in the near infrared (termed B880 after his long-wavelength Q_y absorption peak). Thus, it is believed to have only a single membrane-embedded spectral form of LHC. Other bacteria, like *Rhodobacter (Rb.) sphaeroides,* have more heterogeneous absorption spectra with peaks at 800, 850, and 875 nm. Biochemically, two different LHCs—B800–850 and B875—have been separated. Higher plants have still more complicated antenna buildup. Green bacteria, as well as red and blue-green algae, contain an extramembraneous accessory LHC (chlorosomes and phycobilisomes, respectively) that consists of several spectrally different chromoproteins (for recent review see reference 1).

Excitation migration and trapping processes in spectrally homogeneous antennae, i.e., containing merely spectrally equivalent sites, are qualitatively quite well understood. Theory predicts monoexponential decay of fluorescence (which is one of the inevitable loss channels in photosynthesis, though relatively small) (5, 6). Assuming spatial heterogeneity in the antenna structure (7, 8) or taking into account the charge recombination reaction in RC (9), which results in the reexcitation of the antenna, gives biexponentiality. In any case, antenna fluorescence decay kinetics are independent of the recording wavelength. *R. rubrum* at room temperature behaves very much like predicted above (10).

On the other hand, it is widely accepted that spectrally different groups of LHCs are spatially organized with respect to RC in the order of descending absorption wavelength to develop an energy sink for a more efficient drive of light excitations toward RC (11–14). A large number of kinetic experiments (see, for example, references 15–17, and references therein) provide support for this view of spectrally and spatially directed energy transfer in heterogeneous light-harvesting antenna.

Recent time-resolved fluorescence data (18, 19), revealing spectral dependence of the picosecond fluorescence lifetime in *R. rubrum* at lower temperatures, contradict strongly the predicted homogeneous antenna composition, even in the simplest photosynthetic membranes. In reference 20, the enhancement of fluorescence anisotropy with the increase of the excitation wavelength was disclosed, which also points to the inhomogeneous nature of an *R. rubrum* antenna.

Address correspondence to Dr. Pullerits.

0006-3495/92/10/879/18 $2.00

The probable physical reason for such internal inhomogeneity may be the slight difference of pigment-protein and pigment-pigment interactions in pigment-protein complexes, as well as local dielectric effects of the solvent (lipid surrounding). There is already sufficient experimental evidence that certain kind of static inhomogeneous broadening of optical spectra is a universal property of not only low-temperature solid solutions of relatively simple molecules (21), but of complex biological systems as well. The spectral hole-burning experiments with carbonmonoxymyoglobin (22); bacteriorhodopsin (23); phycobiliproteins (24); Bchl *a* protein from green bacteria (25); B800–850 LHCs of *Rb. sphaeroides* (26); and of higher plants photosystem I (27); photosynthetic RCs (28, 29), and postetiolated maize leaves (30) leave no space for different interpretations. It is also supported by the dependence on the detection wavelength of the rate of the primary electron transfer in RC (31). Therefore, the widespread application of spectrally homogeneous models of excitation transfer and trapping (5–8) to real photosynthetic membranes is hardly justified.

The general theories of nonequilibrium excitation transport in energetically disordered systems (32–36) are not applicable straightforwardly because of some special properties of photosynthetic systems. They also need a mathematical formalism, which makes them hard to be intuitively understood.

In references 13 and 14, simple multicolored models have been worked out. They are valuable to understand the limiting factors of photosynthesis, but due to the lack of internal inhomogeneity of the spectral bands and the arbitrary timescale used, the practical value of these works for the interpretation of real time-resolved experiments (16–19) is quite limited.

In recent articles (37–39), the models have been developed that take into account the fundamental spectral inhomogeneity of photosynthetic systems. A reasonably good agreement between theoretical and experimental kinetics has been demonstrated both at 77 K and at ambient temperatures (39).

In the present paper, we extend and improve the model (39) to describe fluorescence polarization phenomena (20) and to take into account the inner structure of RCs, which gives a weak recombination luminescence in the picosecond emission spectrum (10). These improvements have been published partly already (40). We have also developed an analogous approach for the ultra-low temperature limit. Taking into account more correct spectral parameters for RCs and a photosynthetic unit (PSU) constitution, more consistent with the known structural data, has considerably improved the agreement between the model and the experiment. The PSU structures different from those in reference 39 may even change the qualitative meaning of the antenna spectral inhomogeneity.

The paper is organized as follows. In part II, the basic model and standard approximations used are described and motivated. Then the basic model is extended to make it practically applicable for the interpretation of photosynthetic energy transfer data. In part III, the "operation" of the model and different model predictions are investigated via computer simulations. Comparison with the experimental data is made in part IV. The main results are discussed in part V, leaving conclusions in part VI. Details of the mathematical formalism are given in four appendices.

II. MODEL

Main features

In most of the photosynthetic organisms, the photosynthetic apparatus is embedded into a thin (3–4 nm) cytoplasmic membrane bilayer (1). Energy transport in such a system takes place mainly in two dimensions, as the network of relatively well-ordered (1) LHCs or their complex aggregates (41) extend, for example, in the case of purple bacteria, over the whole chromatophore membrane [a ball of 55 nm diam (42)]. To be specific, we consider a two-dimensional regular arrangement model to be of repeating basic PSUs containing a single RC and a countable number of LHCs in the lattice sites. We suggest that the pigment molecules in LHC are strongly exciton-coupled, and therefore the concrete inner structure of LHC does not have any significant influence on the relatively slow incoherent Förster-type energy transfer between different LHCs and from LHCs to RC (2, 3).

In our model, the RC functions as a shallow trap for singlet excitations of antenna pigment aggregates. Part of the excitations reaching RC move back to the antenna untrapped and part of them photooxidize RC and will this way be used or trapped. The electron is carried from the excited special pair of pigment molecules, P*, of RC, which serve as the main acceptor for antenna excitations, to the sequence of different electron acceptors. In purple bacteria, for example, these are the so-called intermediate electron acceptor bacteriopheophytin (I) and two stable quinone electron acceptors (Q). The radical pair state P^+I^- either gives the electron to the first stable quinone acceptor to form the state P^+IQ^- with lower free energy, recombines to form the ground state P, or returns to form the excited state P*. Back transfer from Q takes place but is too slow and out of time range of our interest.

The master equation, which describes the excitation migration and trapping in PSU with RC in the first lattice site, has the following form:

$$\begin{cases} \dot{p}_i = \sum_{j=1}^{N} (p_j W_{ji} - p_i W_{ij}) - p_i/\tau_1 - \delta_{1i}(p_1/\tau_{RC} - p_0 f/\tau_{RC}) \\ \dot{p}_0 = p_1/\tau_{RC} - p_0(f/\tau_{RC} + 1/\tau_Q) \end{cases} \qquad i = 1 \cdots N \quad (1)$$

Here p_i is the probability that excitation is at pigment-protein complex i, p_0 denotes the radical pair P^+I^- state, $N-1$ is the number of LHCs in PSU, τ_1 is the time of excitation decay due to all the losses in the antenna except quenching by RC, δ_{ij} is the Kronecker delta, τ_{RC} is the charge separation $P^* \rightarrow P^+I^-$ time in RC, τ_Q is the time required for process $P^+I^- \rightarrow P^+IQ^-$ and $f = \exp(-\Delta E_{RC}/kT)$, where ΔE_{RC} is the free energy difference between the states P*I and P^+I^-, k is the Boltzmann constant, and T is the absolute temperature. W_{ij} is the rate of excitation transfer from the site i to the site j.

According to the standard Förster theory (43)

$$W_{ij} = \frac{3}{2}\chi_{ij}^2 \frac{R_0^6}{\tau_0 r_{ij}^6}, \tag{2}$$

where r_{ij} is the distance between the energy donor and acceptor (in our case, lattice sites), τ_0 is the natural fluorescence lifetime of a donor, R_0 is the Förster radius, i.e., the distance at which the energy transfer rate equals the radiative excitation decay rate, and

$$\chi_{ij} = \cos\alpha_{ij} - 3\cos\beta_{ij}\cos\gamma_{ij}. \tag{3}$$

α_{ij} is the angle between the transition dipole moments of the donor i, and the acceptor j, β_{ij}, and γ_{ij} are the angles between each dipole and the vector connecting them.

The higher-order terms in Eq. 1 that describe excitation annihilation processes have been omitted. It is justified when photosynthetic processes under natural low excitation intensities are studied.

Cyclic boundary conditions allow one to consider the possible excitation exchange between different PSUs [the lake model (5)].

This is essentially the basic model, which is quite well understood (5–9).

Spectral inhomogeneity

Let us develop this model, taking into account that the sites are not equivalent and that R_0 needs to be modified. In references 38–40, a temperature-dependent microscopic Förster radius for the excitation transfer from the site i to the site j is introduced to describe the energy migration in the presence of spectral inhomogeneity:

$$R_{ij}^6(\nu_{ij}, T) = R_0^6(0, T_0)\theta_{ij}(\nu_{ij}, T), \tag{4}$$

where $R_0(0, T_0)$ ($\equiv R_0$ in Eq. 2) is the Förster radius defined for a donor and an acceptor with homogeneously broadened spectra at the temperature T_0 if $\nu_{ij} = \nu_i - \nu_j = 0$. ν_i and ν_j denote the transition energies at the sites i and j.

$$\theta_{ij}(\nu_{ij}, T) = F_i \oplus A_j(\nu_{ij}, T)/F_i \oplus A_j(0, T_0). \tag{5}$$

$\oplus$ means convolution:

$$F_i \oplus A_j(\nu_{ij}, T) = \int_{-\infty}^{\infty} F_i(\nu, T)A_j(\nu - \nu_{ij}, T)\,d\nu. \tag{6}$$

$F_i(\nu, T)$ and $A_j(\nu, T)$ are normalized by the area temperature-dependent homogeneous fluorescence and the absorption spectra of sites i and j, respectively.[1]

In Eqs. 2 and 4, the Förster radius is defined for the homogeneously broadened spectra. However, because of the inevitable inhomogeneous broadening, the experimentally determined R_0 may essentially deviate from the ideal $R_0(0, T_0)$, especially in case in vivo situation is analyzed by using in vitro data. How large may the effect be can be demonstrated by simulating the results of the corresponding experiments.

There are two widespread experimental methods for determining R_0: measuring the stationary absorption and fluorescence spectra of pigments and then calculating their spectral overlap or measuring the fluorescence depolarization rate as a function of pigment concentration. As shown in Appendix A, both of them give the same dependence of experimentally observable R_{0E} as a function of the spectral shift between the peaks of the related homogeneous absorption and fluorescence spectra, the homogeneous Stokes shift (HSS) S (44), and of the homogeneous σ_h and inhomogeneous σ_{idf} spectral bandwidths:

$$R_{0E}^6 = R_0^6(0, T_0)\frac{\sigma_h(T_0)}{\sqrt{\sigma_h(T_0)^2 + \sigma_{idf}^2}} \times \exp\left[\frac{S^2\sigma_{idf}^2}{4(\sigma_h(T_0)^2 + \sigma_{idf}^2)\sigma_h(T_0)^2}\right]. \tag{7}$$

Fig. 1 illustrates this dependence, giving the surface of $R_{0E}^6/R_0^6(0, T_0)$, when S and σ_{idf} change in reasonable limits from 0 to 3 and 0 to 8, respectively, relative to the homogeneous bandwidth σ_h.

Clearly, experimental values of Förster radius may considerably deviate from the actual ones. This is the reason why the estimated lattice constant $a = 32$ Å in reference 39 should not be taken too seriously. Actually, the parameter of importance for fitting experimental curves is the nearest neighbor hopping time, which is determined by the ratio $(R_0/a)^{-6}$ and not by R_0 and a separately. It means that corrections of R_0 lead to the change of the estimated lattice constant a, but all qualitative results remain valid. The same comments hold also for another model parameter τ_0, which is ill determined

[1] We note here that all formulas in this work are general and do not depend on the nature of the specific site i that could be either the antenna oligomer or RC special pair. As always in concrete calculations, spectral parameters belonging to appropriate sites have been used.

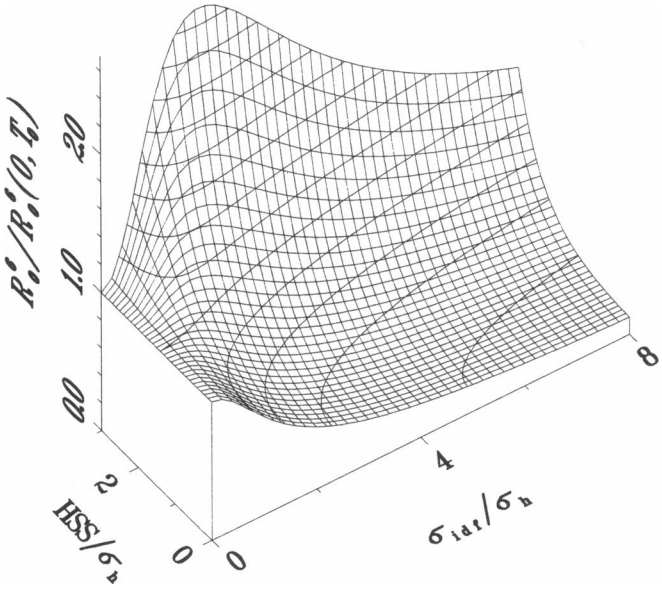

FIGURE 1 Three-dimensional picture that gives the dependence of the sixth power of ratio of experimentally observable Förster radius and resonant Förster radius (see text) on the homogeneous Stokes shift (HSS) and the Gaussian sigma of the IDF σ_{idf}.

because we actually do not know the nature (monomeric chromophore, dimer, or a bigger molecular aggregate) of in vivo antenna site.

After realizing that, we define here the resonant pairwise hopping time between two nearest neighbors at the temperature T_0 (if $\chi^2 = 2/3$):

$$\tau_{hp}(0, T_0) = \frac{\tau_0 a^6}{R_0^6(0, T_0)}, \tag{8}$$

where a is the mean lattice constant in PSU.

Introducing Eq. 8 into Eq. 4 and Eq. 4 into Eq. 2, where R_0 is changed to $R_{ij}(\nu_{ij}, T)$, we have for the modified rate constants

$$W_{ij} = \frac{3}{2}\chi_{ij}^2 \frac{\theta_{ij}(\nu_{ij}, T)a^6}{\tau_{hp}(0, T_0)r_{ij}^6}, \tag{9}$$

where the distance between the lattice sites i and j can be written through a and the mean lattice fluctuation b ($b \ll a$):

$$r_{ij} = l_{ij}a + zb. \tag{10}$$

Here l_{ij} is determined by lattice symmetry properties and i, j; z is a random number between -1 and 1.

If i or j is 1 (it means transfer antenna $\leftrightarrow$ RC), then in Eq. 9 τ_{hp} must be replaced by τ_{hp}^{RC}. Analogously, in case of multiple antenna spectral forms, like in *Rb. sphaeroides*, it is reasonable to expect individual τ_{hp} inside each spectral band and also for transfer between different spectral bands due to changed physical properties of sites.

High-temperature limit

In case of multiphonon transitions (at temperature above or around the Debye temperature, for organics, including proteins, $\geq$100 K), the homogeneous spectra are well approximated by Gaussians (45), and we get

$$\theta_{ij}(\nu_{ij}, T) = \frac{\sigma_{ij}^h(T_0)}{\sigma_{ij}^h(T)} \exp\left[-\frac{1}{2}\left(\frac{(\nu_{ij} - S_{ij})^2}{\sigma_{ij}^h(T)^2} - \frac{S_{ij}^2}{\sigma_{ij}^h(T_0)^2}\right)\right], \tag{11}$$

where $\sigma_{ij}^h(T)^2 = \sigma_i^h(T)^2 + \sigma_j^h(T)^2$, $S_{ij} = (S_i + S_j)/2$. The temperature-dependent full width of the homogeneous spectra of the site i at half maximum intensity (FWHM) is derived as $\Delta_i^h(T) = \sqrt{2 \ln 2}\sigma_i^h(T)$. The HSS of the site i, S_i, can be calculated according to reference 39 by formula

$$S_i = \frac{\Delta_i(T_1)^2 - \Delta_i(T_2)^2}{(8 \ln 2)(T_1 - T_2)k}, \tag{12}$$

where $\Delta_i(T)$ is temperature-dependent experimentally observable FWHM of an inhomogeneous absorption band, which is a convolution of the homogeneous absorption spectrum of the site i, $A_i(\nu, T)$, with the distribution function of electronic transition energies of the sites [the inhomogeneous distribution function (IDF)]. Further on we will assume that $\Delta_i(T)$ and $\Delta_i^h(T)$, which belong to a single antenna system (e.g., B880 in *R. rubrum*), are all equal but different from those of RC site. In the case of a heterogeneous antenna (e.g., B800–850 and B875 of *Rb. sphaeroides*), they may differ for separated antenna pools as well.

Note that S_i could not be measured directly from the spectra as the difference between the fluorescence and the absorption maximum because, due to the energy transfer, the maximum of fluorescence spectrum is shifted to the red (39), and this may lead to remarkable mistakes. It could rather be calculated according to Eq. 12.

In case both homogeneous subbands and IDF have a Gaussian shape, the inhomogeneously broadened absorption band is also a Gaussian with FWHM $\Delta_i(T)^2 = \Delta_0^2 + \Delta_i^h(T)^2$, where Δ_0 is the FWHM of IDF. This relation, together with the temperature dependence of σ_i^h (45)

$$\sigma_i^h(T)^2 = \sigma_i^h(0)^2 + kTS_i, \tag{13}$$

where $\sigma_i^h(0)$ is a temperature-independent constant if $T \gg 0$, $[\sigma_i^h(0) \approx 0]$, sets limits for the reliable values of Δ_0 and Δ_i^h.

Now we are able to calculate the transfer probabilities W_{ij} according to Eq. 9 in high-temperature limit, giving all the sites their energies ν_i within the IDF and transition dipole orientations. It is possible to show that the detailed balance condition is satisfied between forward and backward transitions,

$$W_{ij} = W_{ji} \exp(-\nu_{ji}/kT), \qquad (14)$$

for both transfers, antenna ↔ antenna and antenna ↔ RC.

Low-temperature limit

At zero temperature, the homogeneous absorption and fluorescence spectra consist of a narrow zero-phonon line and a much broader phonon wing (44). $A_i(\nu)$ and $F_i(\nu)$ may be given as in reference 46 by:

$$A_i(\nu) = \varphi_i L_i(\nu - \nu_i) + (1 - \varphi_i) Q_i(\nu - \nu_i) \qquad (15)$$

$$F_i(\nu) = \varphi_i L_i(\nu - \nu_i) + (1 - \varphi_i) Q_i(\nu_i - \nu), \qquad (16)$$

where $\varphi_i = \exp(-S_i/2\hbar\bar{\omega}_i)$, [$\bar{\omega}_i$, a certain average frequency of phonons that interact effectively with the electronic transition at the site i, $S_i/2\hbar\bar{\omega}_i$, is called the dimensionless Stokes losses or the Huang-Rhys factor (44)], L denotes a zero-phonon line of a Lorentzian shape with FWHM Γ_i and a peak at ν_i:

$$L_i(\nu - \nu_i) = \frac{\Gamma_i/(2\pi)}{(\nu - \nu_i)^2 + (\Gamma_i/2)^2}, \qquad (17)$$

and Q is a phonon wing

$$Q_i(\nu) = \begin{cases} (\nu/\mu_i^2) \exp(-\nu/\mu_i) & \nu \geq 0 \\ 0 & \nu < 0. \end{cases} \qquad (18)$$

μ_i determines the shape of the phonon wing: its maximum is situated at $\nu = \mu_i$, the center of weight (the first moment), at $\nu = 2\mu_i$ and FWHM $\approx 2.5\mu_i$.

By using these shape functions, $\theta_{ij}(\nu_{ij}, 0)$ may be calculated according to Eq. 5. Convolution 6 can now be written in a more detailed manner:

$$F_i \oplus A_j(\nu_{ij}) = \varphi_i\varphi_j L_i \oplus L_j(\nu_{ij}) + (1 - \varphi_i)(1 - \varphi_j) Q_i \oplus Q_j(\nu_{ij}) + \varphi_i(1 - \varphi_j) L_i \oplus Q_j(\nu_{ij}) + (1 - \varphi_i)\varphi_j Q_i \oplus L_j(\nu_{ij}). \qquad (19)$$

The first and the second convolution can be calculated analytically (see Appendix B) but the other two have no simple analytical form and should be integrated numerically.

To illustrate what is said above, in Fig. 2 the IDF of RC and the antenna together with the homogeneous fluorescence and the absorption spectrum of one antenna site at the blue edge of antenna IDF and RC special pair at the red edge of RC IDF at 4, 77, and 300 K are given. To get experimentally observable absorption and fluorescence spectra, the convolution of IDF with appropriate homogeneous spectra should be made. In case of antenna fluorescence, the real spectrum may be more red-shifted because of directed energy transfer from higher energy sites to the sites with lower energy (see reference 39).

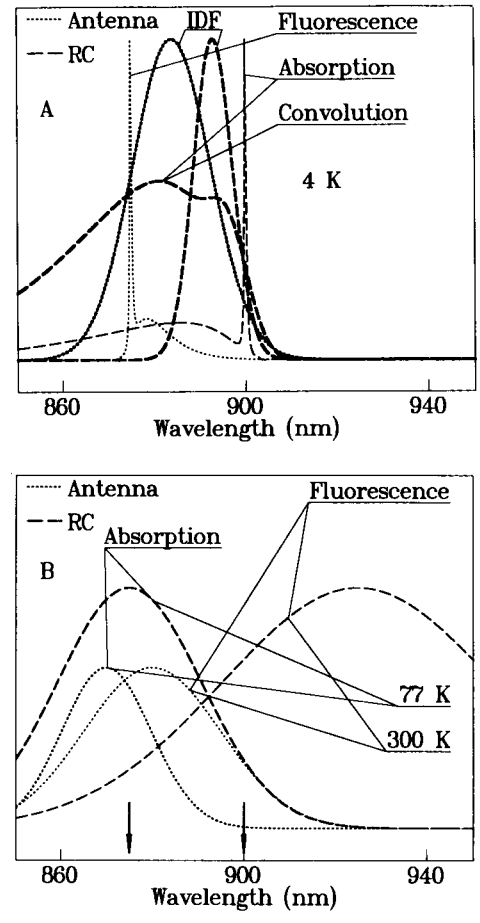

FIGURE 2 The spectra used in model calculations. (*A*) A low-temperature case: inhomogeneous distribution function (IDF) for the antenna LHC and RC; homogeneous fluorescence spectrum of an antenna LHC that absorbs at the blue edge of antenna IDF; homogeneous absorption spectrum of RC situated at the red edge of RC IDF; inhomogeneously broadened RC absorption spectrum that is calculated as convolution of the RC homogeneous absorption spectrum and RC IDF. (*B*) Homogeneous spectra at high temperatures: absorption spectra of antenna LHC and RC at 77 K and fluorescence spectra of LHC and RC at 300 K. Absorption and fluorescence spectra are mirror-symmetric to 0–0 transition, which coincides with sharp zero-phonon-lines at *A*, and are indicated by arrows at *B*. It enables one to get spectra that are not shown. FWHM used at 4 K: antenna IDF, 20 nm = 225 cm^{-1}; RC IDF, 100 cm^{-1}; antenna and RC zero-phonon-line, 5 cm^{-1}; phonon wing for antenna, 100 cm^{-1}; for RC, 400 cm^{-1}. At 77 K: the homogeneous antenna spectrum, 23 nm = 260 cm^{-1}; the homogeneous RC spectrum, 38 nm = 430 cm^{-1}. At 300 K: the homogeneous antenna spectrum, 35 nm = 400 cm^{-1}; the homogeneous RC spectrum, 70 nm = 800 cm^{-1}.

Green function approach to the master equation

It is possible to transform master Eq. 1 into a more compact form:

$$\dot{\mathbb{P}}(t) = \mathbb{R}\mathbb{P}(t). \qquad (20)$$

$\mathbb{P}(t)$ is the vector of site occupation probabilities and $\mathbb{R}$ is the $(N + 1) \times (N + 1)$ rate matrix. By using the Green

function formalism as in reference 37, the solution of the set of coupled first-order differential equations can be written as

$$\mathbb{P}(t) = \mathbb{G}(t)\,\mathbb{P}(0), \tag{21}$$

where $\mathbb{P}(0)$ is the vector of initial distribution of excitations created by optical absorption and the Green function $\mathbb{G}(t)$ is given by

$$\mathbb{G}(t) = \mathbb{M}^{-1} \exp(\lambda t)\mathbb{M}, \tag{22}$$

where $\mathbb{M}$ is the matrix of eigenvectors and $\lambda = \mathbb{M}\,\mathbb{R}\,\mathbb{M}^{-1}$ is the diagonal matrix of eigenvalues. The matrix elements $G_{ij}(t)$ are interpreted as the conditional probability that an excitation starting at site j at $t = 0$ will be found on the site i at the time t. Thus, $\mathbb{G}(t)$ evolves the initial distribution of excitations into the distribution at the time t.

If the Green function, homogeneous absorption, and fluorescence spectra of the sites are known, then it is possible to calculate the dependence of isotropic fluorescence kinetics $I(t)$ as a function of the exciting and recording frequencies:

$$I(\nu_{exc}, \nu_{rec}, t) = \mathbb{F}(\nu_{rec})\mathbb{G}(t)\mathbb{A}(\nu_{exc}), \tag{23}$$

where $\mathbb{F}(\nu_{rec})$ is the vector of site fluorescence intensities at the recording frequency ν_{rec} and $\mathbb{A}(\nu_{exc})$ is the vector of site absorption coefficients at the exciting frequency ν_{exc}.

Eq. 23 represents the sum of exponentials

$$I(\nu_{exc}, \nu_{rec}, t) = \sum_{i=0}^{N} C_k(\nu_{exc}, \nu_{rec}) \exp(\lambda_k t), \tag{24}$$

where $C_k(\nu_{exc}, \nu_{rec})$ are given by

$$C_k(\nu_{exc}, \nu_{rec}) = \left[\sum_i F_i(\nu_{rec}) M_{ik}\right] \sum_j M^{-1}_{kj} A_j(\nu_{exc}). \tag{25}$$

Time integration of Eq. 23 gives the steady-state fluorescence spectrum:

$$I(\nu_{exc}, \nu_{rec}) = \mathbb{F}(\nu_{rec})\tilde{\mathbb{G}}\mathbb{A}(\nu_{exc}), \tag{26}$$

where $\tilde{\mathbb{G}} = \mathbb{M}^{-1}\mathbb{T}\mathbb{M}$. $\mathbb{T}$ is the diagonal matrix of negative reciprocals of the eigenvalues of the rate matrix $\mathbb{R}$. In other words, $\mathbb{T}$ is a diagonal matrix of decay constants.

Polarization

Besides the isotropic fluorescence in Eq. 24, it is also possible to derive analogous equations for fluorescence profiles $I_{\parallel}(\nu_{exc}, \nu_{rec}, t)$ and $I_{\perp}(\nu_{exc}, \nu_{rec}, t)$ polarized parallel and perpendicular to the excitation polarization $\vec{e}$. Preexponential coefficients are then given by (see Appendix C):

$$C^{\parallel}_k(\nu_{exc}, \nu_{rec}) = \sum_i \left[F_i(\nu_{rec}) M_{ik} \sum_j M^{-1}_{kj} D_{ij} A_j(\nu_{exc})\right], \tag{27}$$

where $D_{ij} = 1 + 2\cos^2 \alpha_{ij}$, and

$$C^{\perp}_k(\nu_{exc}, \nu_{rec}) = 2.5C_k(\nu_{exc}, \nu_{rec}) - 0.5C^{\parallel}_k(\nu_{exc}, \nu_{rec}). \tag{28}$$

If the distribution of the orientations of transition dipole moments is known, it is possible to integrate D_{ij} over that distribution. In the case of random orientation in space or plane, we have, respectively,

$$D_{ij} = \begin{cases} 3 & i = j \\ 2 & i \neq j. \end{cases} \tag{29}$$

For stationary emission polarized parallel and perpendicular to $\vec{e}$, we get

$$I_{\parallel}(\nu_{exc}, \nu_{rec}) = \sum_{i,j} F_i(\nu_{rec}) D_{ij} \tilde{G}_{ij} A_j(\nu_{exc}) \tag{30}$$

$$I_{\perp}(\nu_{exc}, \nu_{rec}) = 2.5I(\nu_{exc}, \nu_{rec}) - 0.5I_{\parallel}(\nu_{exc}, \nu_{rec}). \tag{31}$$

III. SIMULATIONS

To prove the working power of our model, numerous model simulations have been performed with different initial conditions and parameters of the model. Apart from the Green function method, master Eq. 1 is also solved by the method of Monte Carlo (see Appendix D). Discrepancy of results of different routines is not exceeding 5%. This is less than the uncertainties of experimental results (18, 19) that we are going to analyze in the next part. It should be noted that the 5% difference is determined by a number of Monte Carlo iterations and is not the measure of the model preciseness.

Parameters

Happily enough, most of model parameters can be fixed thanks to the availability of independent and reliable experimental data.

FWHM of the absorption spectrum of *R. rubrum* membrane preparations at room temperatures, at 77 K, and at 4 K is ≈40, 30, and 20 nm with the peaks at 880, 895, and 900 nm, respectively (20, 47, 48). From Eq. 12 we get $S = 10$ nm for high temperature limit. This is about half as large as estimated from the difference of the maxima of the absorption and the fluorescence spectrum. As shown in reference 39, the fluorescence spectrum of chromatophores may be shifted more to the red due to energy transfer. Integrated over the whole band fluorescence decay times of isolated LHC in buffer solution, $\tau_1 = 920 \mp 40$ ps at 4 K, 680 ∓ 30 ps at 77 K, and 635 ∓ 15 ps at 300 K (19).

The RCs from *R. rubrum* and *Rb. sphaeroides* are known to have very similar properties, but the latter ones have been studied more extensively. We assume that the electron transfer and the electron-phonon interaction parameters obtained for *Rb. sphaeroides* are correct also

for *R. rubrum* RCs: $\Delta E_{RC} = 0.16$ eV at 300 K and 0.05 eV below 100 K (49); $\tau_Q = 200$ ps at 300 K and 100 ps below 100 K (50); $\tau_{RC} = 1.2$ ps at 4 K, 1.5 ps at 77 K, and 2.8 ps at 300 K for RCs in the photoactive (open) state (51). In *R. rubrum*, the most long-wavelength absorption band of RC complexes peaks at 870, 885, and 900 nm, respectively, at room temperature, at 125 K and at 4 K, the corresponding FWHM being 70, 45, and 35 nm (52–55). Equation 12 gives for high-temperature case $S = 50$ nm, which is in a good agreement with the experimental Stokes shift between the RC absorption and fluorescence maxima (56). Extrapolating the reported data to 77 K, we have taken the FWHM $\approx$ 38 nm and the absorption band maximum at 890 nm.

In reference 39, to suit the experimental data at low temperatures, the RC absorption band maximum had to be too much red-shifted (to ~905 nm at 77 K) in comparison with the known literature data. Even then the nonrandom antenna organization able to funnel the energy toward RC had to be assumed. In reference 39, for simplicity the same bandshapes were taken for both of the antenna sites and the RC primary donor P870. It leads, as we have shown before, to underestimation of RC HSS by a factor of about five (instead of 50 nm, 10 nm). Also, because of the much wider homogeneous spectra that RC has compared with the antenna, the function $\theta_{ij}(\nu_{ij}, T)$ is also wider for the transition antenna $\leftrightarrow$ RC compared with the transition antenna $\leftrightarrow$ antenna, and even if there is an energetically uphill transfer to RC, the transfer efficiency is still quite high. It is illustrated by Fig. 3, where the dependence of θ_{ij} on ν_{ij} and T is given for both antenna $\leftrightarrow$ RC and antenna $\leftrightarrow$ antenna transfers.

Direct calculations evidence that the broad homogeneous spectrum of P870 has a fundamental significance. It makes the energy transfer from the antenna to the RC sufficiently efficient also in the case of a core antenna with reasonable spectral disorder.

Calculations for *Rhodopseudomonas* (*Rps.*) *viridis* with parameters obtained from fitting the *R. rubrum* experimental curves (see below) agree quite well with the value revealed by electric measurements (57).

The homogeneous spectral characteristics at low temperature limit were estimated from hole-burning experiments, though for RC quite contradictory results have been presented (for review see reference 58). The recent data (55) give for *Rb. sphaeroides* RCs $\Gamma = 5$ cm^{-1}, HR = 2, 2.5 $\mu \approx 400$ cm^{-1}, and $\Delta_0^{RC} \approx 100$ cm^{-1}, and they have been put into the model.

For bacterial antenna, very few data are available (26). Assuming that electron-phonon coupling parameters are nearly the same in case of antenna bacteriochlorophyll-proteins and chlorophyll-proteins, the results obtained in PS-I particles (27) and in greening leaves (30) are taken into account in our calculations. The zero phonon line Γ is taken equal to 5 cm^{-1} (the exact value of this parameter has far less influence on excitation

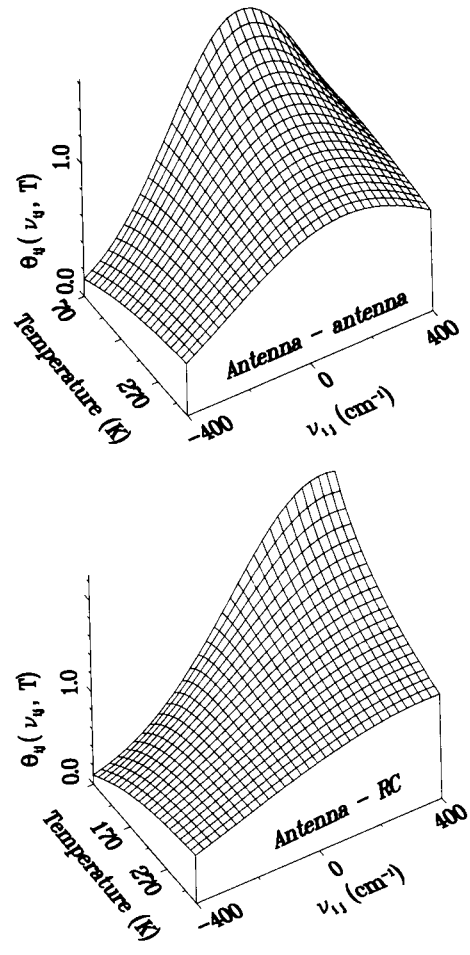

FIGURE 3 Dependence of the transfer rate on the energy difference ν_{ij} and temperature, relative to the rate at 300 K if $\nu_{ij} = 0$. Two surfaces give the transfer between two antenna LHCs and between LHC and P.

transfer rates than HR and μ do), HR $\approx$ 0.8 and FWHM of phonon wing 2.5 $\mu \approx 100$ cm^{-1}.

In the following, if not stated otherwise, these parameters are used.

So, the only adjustable parameters of the model, which one has to estimate from comparison with the experiment in case of the specific PSU structure (see below), are the pairwise hopping times τ_{hp}, τ_{hp}^{RC} and FWHM of antenna IDF.

Structure

As a rule, pigments in photosynthetic pigment-protein complexes are strongly aggregated (1). Transition dipole moment of the aggregate consisting of N identical molecules is equal to $\sqrt{N}\vec{d}$, where $\vec{d}$ is the transition dipole moment of a single molecule (59). This dependence on N becomes saturated when the aggregate size becomes comparable with the wavelength of the light associated with the optical transition. $\sqrt{N}\vec{d}$ dependence is the result of a coherent interaction of all the molecules in the aggregate with the radiation field. Inhomogeneous distri-

bution of the transition frequencies of the constituents of the aggregate does not affect intermolecular coherence until the interaction between molecules inside of the aggregate is much larger than the width of IDF. High temperature destroys coherence between different molecules and the effective number of coherently coupled molecules $N_{eff} \rightarrow 1$ as the dephasing rate becomes sufficiently large (60).

$\sqrt{N}$-dependence, like the increase in Q_y dipole strength at the expense of the Soret band (hyperchromism) (61), leads to a more efficient energy transfer to RC (62). Energy transfer kinetics is dependent also on the mutual positions of LHCs as well as LHCs and RC. Unfortunately, the exact composition of membrane-embedded PSUs is not yet well determined. The experimental data available are not all convergent.

Gingras and Picorel (63) studied B880 of *R. rubrum* by radiation inactivation and electron paramagnetic resonance, concluding that B880 consists of hexameric aggregates of protein α,β-polypeptide pairs binding Bchls, which force the 12 Bchl molecules to form closed assemblies. In the PSU of *R. rubrum,* there are $\approx$24 Bchl antenna molecules per RC (64). It means that there must be no more than two to three LHCs per RC. On the contrary, in references 65–67, relying on electron microscope data, the hexagonal structure of PSU has been proposed for both *R. rubrum* and *Rps. viridis*. Besides, it was found lately that the *R. rubrum* B880 LHCs could be reversibly dissociated into the so-called B820 subunit form (68). The most probable composition of this complex has been reported to be $\alpha\beta$(Bchl $a)_2$. A study of reassociation of these subunits (69) strongly suggests the reaction scheme 2 B820 → B880 and a basic unit of B880 that consists of four Bchl *a* molecules as proposed in reference 1.

We will assume here a core antenna model with six antenna LHCs per RC, each containing four Bchl *a* molecules. Molecules in this aggregate are so strongly coupled that the excited states are delocalized over all substituent molecules, forming a kind of supermolecule. This supermolecule is characterized with a single near infrared dipole-allowed electronic transition. We also assume that energy transfer between different aggregates is describable by the Förster mechanism. $\sqrt{N}$-dependence is included indirectly through τ_{hp}, which is one of the model parameters determined from comparison with the experiment.

To better understand the relationship between the structure and excitation migration and trapping kinetics, calculations with three different PSU geometries have been performed (see Fig. 4). The structure *A* in Fig. 4 is a square lattice, and *B* and *C* represent two differently packed hexagonal lattices.

As we saw above (Eq. 24), the fluorescence kinetics can be represented as a sum of exponentials. By fixing the exciting wavelength, Eq. 24 can be written in a more generalized way:

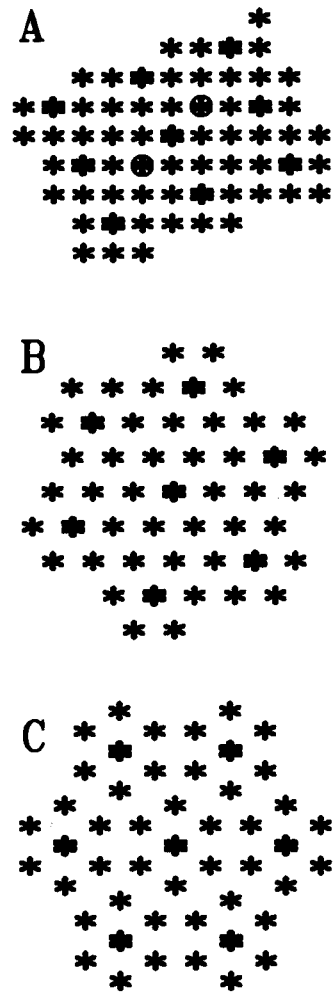

FIGURE 4 The model lattices in case there are six LHCs in a PSU. The bold asterisks are RCs. Two circled LHCs in the central PSU of the case *A* have no RCs among the nearest neighbors.

$$I(\nu_{rec}, t) = \int_0^\infty \rho(\nu_{rec}, \tau) \exp(-t/\tau)\, d\tau, \qquad (32)$$

where $\rho(\nu_{rec}, \tau)$ is the distribution of amplitudes of fluorescence decay constants at the emission frequency ν_{rec}.

In Fig. 5, the $\rho(\tau)$ (a homogeneous antenna was assumed where there is no dependence of ρ on ν_{rec}) for three different antenna structures shown in Fig. 4 are given. Here and in the following, if not stated otherwise, room temperature, open RCs, $\chi^2 = 2/3$, $\tau_{hp} = 60$ ps, and $\tau_{hp}^{RC} = 70$ ps have been used. RC absorption maximum within a Gaussian RC IDF (FWHM = 100 cm^{-1}) is chosen by a random number generator. For convergent results, $\geq$600 different spectral configurations are used. Master Eq. 1 is solved for each configuration, and the corresponding $\rho(\tau)$ are added up.

As one can see, in all three cases we have broad decay time distributions below 100 ps due to the antenna quenching by open RCs and a narrow one of relatively

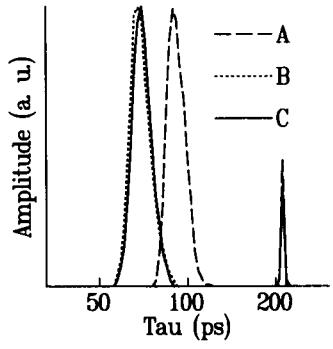

FIGURE 5 Distributions of amplitudes of fluorescence decay constants τ at room temperature for the three different model lattices shown in Fig. 4.

low integral intensity above 200 ps, which is due to the recombination of P^+I^-. One third of the sites in the square lattice (surrounded by circles in central PSU in Fig. 4 *A*) are farther away from the RC than the nearest neighbors, which makes the quenching notably less efficient. Two hexagonal structures have almost the same kinetics but, as the structure *B* is more tightly packed (in *B* each antenna site has six nearest neighbors instead of the five in *C*), the quenching is somewhat more efficient. In the following the PSU structure *C* has been used.

In reality, the antenna array is not probably so well organized. The influence of structural distortions (look member *zb* in Eq. 10) was analyzed in references 40 and 70). We refer the reader to these sources, noting here only that lattice fluctuations may have a very strong influence on decay times.

Orientation

To investigate the anisotropic effects of energy transfer, each site was attributed a specific Q_y transition dipole moment orientation, and χ^2 in the W_{ij} Eq. 9 was calculated according to Eq. 3.

Transition dipole moment of RC special pair is known to be in the membrane plain (71). In *Rps. viridis,* the antenna transition dipole moments are randomly oriented in the membrane plain (72). To the best of our knowledge, there are no data of this kind available about the orientation of antenna dipoles in *R. rubrum;* thus, three different cases have been simulated in the case of model PSU structure C considered in the last paragraph: antenna dipoles are (I) random in space, (II) random at membrane plain, or (III) oriented in the same direction as the RC transition dipole moment (because of the cyclic boundary conditions, it means that all transition dipoles of the whole array are parallel and in the membrane plain).

Fig. 6 gives $\rho(\tau)$ for these three cases. To see the pure action of the orientational disorder, the spectra of both LHC and RC are considered only homogeneously broadened. 1,000 different sets of PSU orientations have been generated in each case.

Again, there is a peak of recombination luminescence around 200 ps and the bands corresponding to the antenna quenching by open RCs. Case III represents a fully ordered PSU, and there are only sharp peaks around 40 and 200 ps. The orientational disorder broadens the τ distributions and makes quenching less efficient, most remarkably in case I. Actually, the integrals $\int \rho(\tau)\, d\tau$ should be equal (note the logarithmic τ scale). It means that curves II and particularly I are overamplified in comparison with I. Therefore, also the short τ components, which denote migration in the antenna, become observable. These components are very weak in case of a homogeneous antenna, because almost every decay component of a site is compensated by the rising component of another site.

Nanosecond component

When the RCs are in the PIQ_A^- state and the electron transfer from I to Q_A after a radical pair P^+I^- formation is blocked, in addition to the main 60–80 ps lifetime fluorescence, a low-amplitude emission component that decays within several nanoseconds has been observed both at room temperature and 77 K (10). The latter is considered to represent a recombination luminescence according to the following scheme: $P^+I^-Q_A^- \rightarrow P^*IQ_A^- \rightarrow PIQ_A^- +$ photon. In case of PS II particles, an alternative interpretation for the origin of the increased fluorescence yields (variable fluorescence) and the appearance of nanosecond lifetime on reduction of Q_A is proposed (73). The negative charge of the quinone acceptor decreases the rate constant of the charge separation τ_{RC} and, according to reference 73, this is the only reason of the variable fluorescence. Our simulations have convinced us that in case of purple bacteria the decrease of τ_{RC} could hardly cause the whole experimentally observable nanosecond decay component (10), and the possible recombination should be considered.

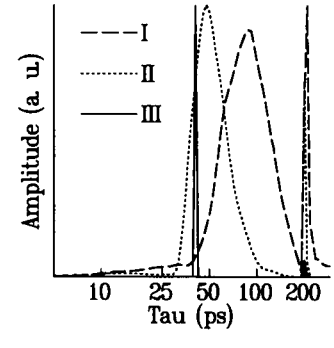

FIGURE 6 Distributions of amplitudes of fluorescence decay constants for three different transition dipole moment orientation distributions in case of model lattice C from Fig. 4. I, random in space; II, random in membrane plane; III, parallel to the RC special pair P transition dipole moment orientation.

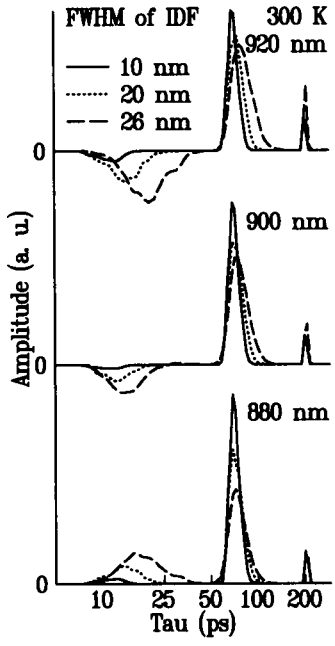

FIGURE 7 Distributions of amplitudes of fluorescence decay constants for three different FWHM of antenna IDF at three recording wavelengths. Temperature is 300 K. Excitation into blue edge of absorption band.

Antenna IDF

The antenna site transition energies within IDF are given by a Gaussian random number generator. 1,000 different randomly generated PSUs were calculated, and the results added up. Because of the cyclic boundary conditions used, in every single calculation out of 1,000 we have a membrane with endlessly repeated identical PSUs. In reality, IDF characterizes the whole membrane and PSUs are different. Check-up calculations assured us that the mistake given by this approximation is insignificant.

Figs. 7 and 8 show the τ distributions at 77 and 300 K in case of photoactive RCs at different recording wavelengths (at the band maximum, on the high- and low-energy slope) and antenna IDF widths: Δ_0 = 10, 20, and 26 nm. Excitation takes place with a weak picosecond light pulse at the blue edge of the absorption band.

At 300 K at all wavelengths, the 200-ps recombination component and 60-ps trapping component can be well recognized. Additionally, the fast 10- to 20-ps component appears as a decay in the blue and as a rise component with negative amplitude in the central and the red part of the fluorescence band. This time reflects hopping between spectrally different antenna sites. This fast component as well as the recombination luminescence component have not been revealed experimentally at room temperature where a single-exponential decay was observed (10). In the former case, the reason is that ideal exciting conditions are used here. If nearly all antenna sites (not only the most blue-absorbing ones) are excited simultaneously as in the experiment, the fast component almost smooths down. The recombination luminescence is presumably too weak to be observed at limited signal-to-noise ratio of the experiment.

At 77 K, the fast component is much more evident and cannot be ignored experimentally. In general, when the IDF broadens, the lifetime amplitude distribution widens as well. However, there is no systematic change of the shape of the amplitude spectrum. We only note that the long decay times (100–200 ps) seen at 930 nm in case of the broadest IDF are due to localization of excitation at the antenna sites of the lowest energies. Energy transfer from those sites to RC slows down at 77 K. The very weak recombination luminescence at such low temperature is cancelled to see more clearly the effect of excitation localization due to antenna IDF. One can see that the energetically random antenna enables sufficiently efficient harvesting of light excitations also in case of relatively large spectral inhomogeneity of site transition energies.

IV. COMPARISON WITH THE EXPERIMENT

Fluorescence kinetics

R. rubrum was chosen as a model system for comparison of the theory and experiment.

According to references 18 and 19, the *R. rubrum* fluorescence kinetics at low temperatures depend on observation wavelength in case of both closed and open RCs. Fitting the experimental results with the theoretical fluorescence kinetics obtained by using the excitation condi-

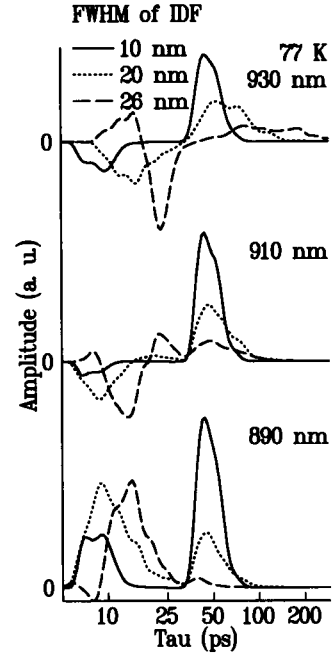

FIGURE 8 The same as Fig. 7 except at 77 K.

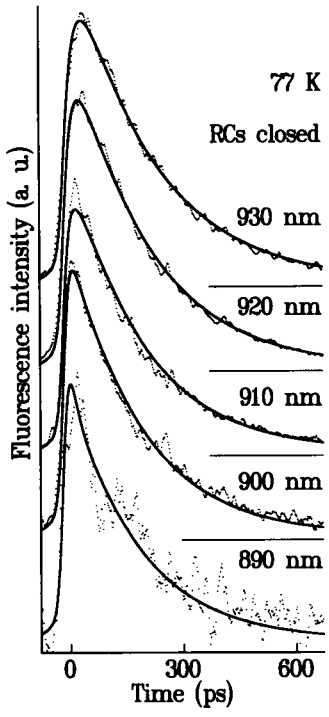

FIGURE 9 Comparison of theoretical kinetics (——) with the experiment (· · ·) at 77 K. RCs in the closed (P photooxidized) state. Excitation at 800 nm excites RC and antenna with equal probabilities. All antenna LHCs are initially equally excited. Δ_0 = 20 nm, τ_{hp} = 60 ps, τ_{hp}^{RC} = 330 ps.

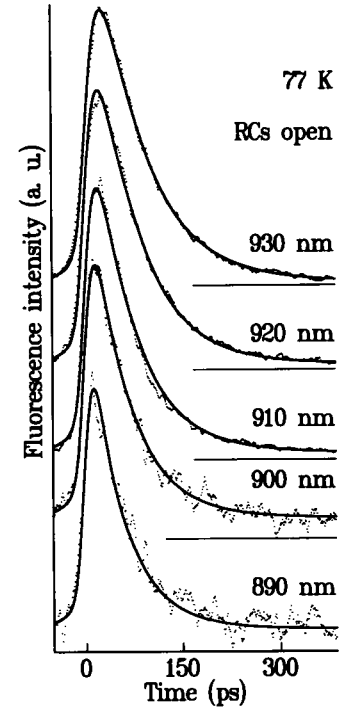

FIGURE 10 The same as Fig. 9 except RCs in the open state. τ_{hp}^{RC} = 70 ps.

tions similar to the experimental ones allows one to estimate the values of adjustable parameters of the model—τ_{hp}, τ_{hp}^{RC}, and Δ_0.

We have found that the initial fast decay most distinctly observed at low temperatures at the blue edge of the fluorescence band is mainly the function of τ_{hp}. Fixing τ_{hp} in that way, τ_{hp}^{RC} is estimated from the longer decay time at the red edge of the spectrum. Then Δ_0 is estimated from the amplitude spectrum of different decay components. After that, the next iteration is made starting again with τ_{hp}, etc.

Figs. 9 and 10 represent 77 K experimental fluorescence decay curves together with the model ones that are convoluted with the experimental instrument response function in case of closed and open RCs, respectively. The following parameters were used: Δ_0 = 20 nm, τ_{hp} = 60 ps, τ_{hp}^{RC} = 70 ps in the case of open RC. The value of τ_{hp}^{RC} was changed to 330 ps for closed RCs, and recombination luminescence was assumed to be negligible.

With the same set of parameters that have been optimized at 77 K (except τ_{hp}^{RC} in case of closed RCs), the room temperature kinetics were satisfactorily reproduced as well (Fig. 11). In case of closed RCs, τ_{hp}^{RC} = 170 ps instead of 330 ps at 77 K has been used.

At 4 K, the fixed value of Δ_0 estimated above has been used, τ_{hp} and τ_{hp}^{RC} being adjustable parameters. By varying these and also some other parameters in reasonable limits, no satisfactory results were obtained. Fig. 12 gives the experimental and model curves when τ_{hp} = 50 ps and τ_{hp}^{RC} = 100 ps at 4 K.

By dividing τ_{hp} by the number of the nearest neighbors, one can estimate the average time the excitation stays at the antenna site between two jumps. This residence time in the antenna site is ~12 ps. We stress that it is the mean residence time. In each case, the time is dependent on the spectral properties of the neighboring antenna sites and may differ from that value considerably.

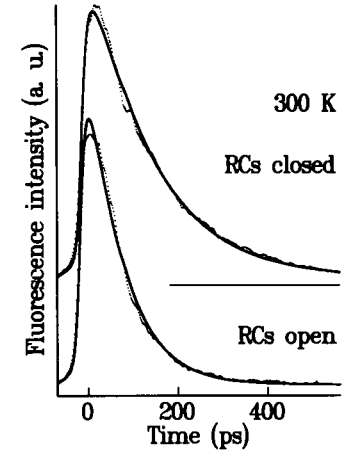

FIGURE 11 The same as Figs. 9 and 10, except at 300 K. τ_{hp}^{RC} = 170 ps in case of closed RCs.

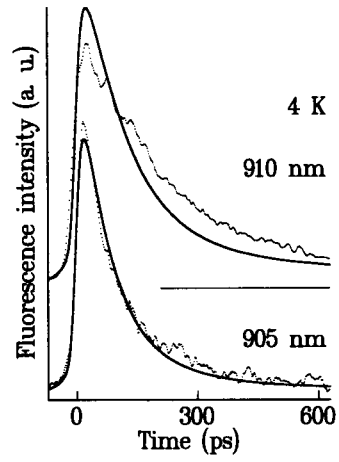

FIGURE 12 The same as Fig. 9, except at 4 K. τ_{hp} = 50 ps, τ_{hp}^{RC} = 100 ps.

In our model, we do not take into account the possible change of the transition frequency of the molecule within IDF after being excited (the mechanism of nonphotochemical hole burning). As the excitation lies preferably on the red part of IDF, this change reduces the number of red molecules, and thus τ_{hp} and the value 12 ps may be slightly overestimated.

The distance between two antenna sites estimated in references 66 and 67 for *Rps. viridis* are 40 and 32 Å, respectively. Taking τ_0 = 18 ns and τ_{hp} from our estimation, it is possible to make an assessment of R_0 for antenna aggregates. From Eq. 2 we get $R_0 \approx 105$ Å or 85 Å for r_{ij} = 40 Å or 32 Å, respectively. Nevertheless, the true τ_0 in in vivo aggregates is unknown and may considerably differ from τ_0 of Bchl *a* in solutions, for example, due to possible superradiance effects of the aggregates (59).

Fluorescence polarization

In reference 20, the enhancement of fluorescence polarization p,

$$p(\nu_{exc}) = \frac{I^{\parallel}(\nu_{exc}) - I^{\perp}(\nu_{exc})}{I^{\parallel}(\nu_{exc}) + I^{\perp}(\nu_{exc})}. \quad (33)$$

with the increase of the excitation wavelength was disclosed at 4 K in *R. rubrum*.

With the assumption of random transition dipole moment orientation of sites, $p(\nu_{exc})$ was calculated at 4, 77, and 300 K by using the parameters derived in the previous section (Fig. 13). Recording wavelengths at different temperatures are denoted by arrows. As one can see, qualitatively the low-temperature experimentally observed effect is well reproduced (see also reference 40), but the calculations show a considerable enhancement of fluorescence polarization even at room temperature. In reference 20, only a slight rise of the polarization curve has been observed, the numerical value of p being also lower. In case of open RCs, p is always larger than for closed RCs due to the shorter fluorescence lifetime and, consequently, less efficient depolarization. The slight increase of p with the decreasing of excitation wavelength in case of open RCs at 77 K is caused by RC absorption. As the absorption and fluorescence spectra of RCs and LHC are shifted with respect to each other at the blue edge of the absorption spectrum, RCs absorb relatively stronger, and yet at the recording wavelength 930 nm they have also a remarkable fluorescence intensity (see Fig. 2). The emission of directly excited RCs is highly polarized and, therefore, p increases at excitation wavelengths below 875 nm. This effect is absent in case of closed RCs because closed RCs do not emit.

V. DISCUSSION

Despite the qualitative agreement between experiment and theory, the failure of the model to fit quantitatively the experimental curves at the low temperature limit provoked us to find out possible oversimplifications in the model and to look for alternative interpretations.

First, unfortunately, very little is known about the real buildup of PSU even in case of simplest photosynthetic systems, like the one analyzed here.

How important it is to know the true number of LHC per RC in PSU and the PSU structure can be illustrated by comparing the results of this work with the data of our previous model simulations (39–40), where the PSU consisting of 19 LHC per RC in square lattice has been considered. In both cases, nearly the same stoichiometric ratio of protein-bound light-harvesting antenna Bchl *a* molecules per RC was assumed. Not only are the pairwise exciton hopping rate and other parameters considerably altered [for example, $\tau_h \approx$ 50–60 ps (this work) and 20–30 ps (39–40)], but also the trajectory of exciton hopping in PSU, the nature of exciton trapping in RC, and even the character of inhomogeneity change essen-

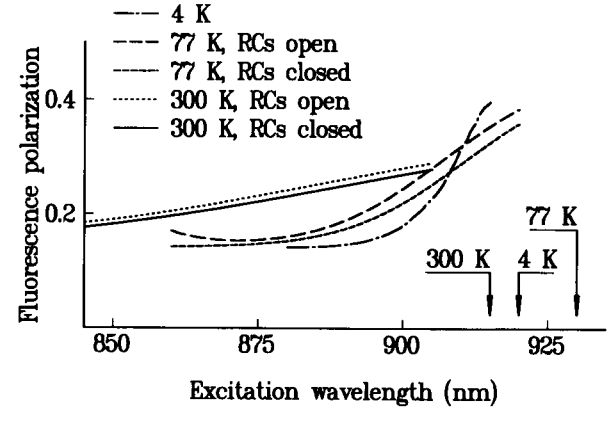

FIGURE 13 The dependence of the degree of fluorescence polarization on excitation wavelength at different temperatures and RC states. Recording wavelengths at different temperatures are denoted by arrows.

tially (see also reference 7). There is a natural limit for the number of LHC per RC when all antenna Bchls in PSU are gathered into a single LHC. Even in this seemingly simple case, there is no straightforward procedure (without computer simulations) to decide whether to keep or discard this model. Qualitatively, when the inner structure of a LHC is still being ignored, the spectral inhomogeneity in such a single-LHC PSU can be imagined as LHCs (and RCs) belonging to different PSUs that have different spectra. Then the hopping time corresponds to the exciton hopping between LHC in the neighboring PSUs and the trapping time preserves its previous meaning. If the inner structure of LHC is taken into account and if the antenna Bchls within an aggregate are only loosely bound, we almost reproduce the situation treated in references 39–40 (there energy transfer between Bchl dimers has been considered). When, however, Bchls within LHC interact strongly revealing complicated homogeneous spectrum, only a concrete analysis has sense.

In our previous work (39), the spectral inhomogeneity was chosen to form an energy funnel toward RC; in this work we have no need to use that kind of energy sink. In both cases the models work reasonably well, especially near photosynthetic temperatures. It is impossible to select the true one by relying only on spectral and kinetic measurements. A more thorough understanding of the fundamental processes of light harvesting and use can be reached by studying energy transfer in the systems for which more detailed structural information is available (74).

Another serious shortcoming, also connected to the shortage of structural information, is the total ignoring of the inner structure of LHC. Actually, four strongly coupled Bchl *a* molecules in LHC may generate four exciton states with different energies, like in case of Bchl *a* protein from green bacterium (25). It means that homogeneous spectra used are not appropriate for quantitative analysis.

The inner structure gives also the possibility to interpret the fast lifetime component as the relaxation from the higher energy states to the lower ones. In reference 75, this possibility is discussed in the case of phycobiliproteins for the decay times of several tens of picoseconds.

Exciton motion immediately after short-pulse excitation may be quite coherent at low temperatures (76). To take this coherence into account, the generalized master equation (77) must be used instead of Eq. 1 at 4 K.

In references 20 and 78, the existence of two antenna spectral forms, a major and a minor, in *R. rubrum* has been proposed. Recent model calculations (79) show that the minor component does not lead to better trapping probability, as it was suggested. This is also inconsistent with the experimental data (19), demonstrating the necessity of at least three components to interpret fluorescence decays at 4 K. It should be noted that the three best-fit time constants found in reference 19 vary systematically with the detection wavelength, in contrast to what is expected if the actual process responsible for the spectral evolution were the interconversion of only two (three) emitting spectral forms. We believe that interpretation in terms of spectral inhomogeneity given by us is more physical and experimentally as well as theoretically well supported. In reference 17, the experiment was also interpreted in terms of the existence of only two different types of B800–850 LHC in *Rb. sphaeroides,* which have different spectral and kinetic properties. We think that in reality there is a continuous distribution of B800–850 LHCs with different coupling to B880 complexes.

As we have seen from simulations, in case of complex biological systems the existence of only a few well-separable fluorescence decay components is unlikely. More or less broad lifetime distributions ordinarily emerge. Relatively good fits of experimental kinetics obtained by using as few as two to three decay components are due to low experimental accuracy and fundamental fallacy in fitting the decay curves (80). As a rule, the physical interpretation of results is not trivial, and comparison with model calculations is necessary.

In most cases the excitation energy in large organic molecules is very rapidly (<1 ps) redistributed over the vibrational manifold of the whole molecule. This nonequilibrium distribution of the vibrational energy (transient internal temperature of the excited molecule) dissipates via interaction with the surrounding solvent molecules. There are many indications that in case of large molecules the intramolecular energy redistribution is faster than the rate at which the excess vibrational energy in the solute molecule is dissipated into the solvent thermostat (inc. protein moiety) (81). Time constants around 10–25 ps were observed for dye molecules and for polycyclic aromatic molecules (82). Transient spectra of heme proteins (carbonmonoxy hemoglobin) have been interpreted in terms of vibrationally hot heme that cools down substantially in 10 ps (83). This result is consistent with molecular dynamic calculations (84) and suggests that the effect of molecular heating should be very seriously considered when interpreting transient spectral changes of chromatophores in picosecond time domain. Moreover, in reference 85 it is shown that vibrationally hot porphyrins cool down by 10 ps.

In our experiments, typically a 800-nm excitation was used (18, 19). The energy that is heating a Bchl *a* molecule in the excited electronic state before dissipating to the surrounding is 1,200–1,300 cm^{-1}. Classically, the thermal energy E of a system of N atoms is expressed as $E = 3NkT$, which gives a temperature rise of ≈ 5 K. It is almost unnoticeable at room temperature. The vibrational frequencies of Bchl *a* are not exactly known in the excited electronic state, but it is reasonable to assume that the room temperature does not represent the classical limit for high-frequency modes. So, the actual temper-

ature rise may be somewhat higher. At low temperature the heat capacity decreases rapidly toward zero temperature, and the temperature rise may several times exceed that at room temperature. On the other hand, in the model of LHC, where four Bchl *a* molecules are in a close energetic contact and they form a big quasimolecule, the expected temperature rise is four times less.

Relying on the data at hand, it is impossible to exclude completely a possibility that at low temperatures the recording-wavelength-dependent fluorescence kinetics in 10–30 ps time domain (18, 19) reflects partially the temperature equilibration process between the excited pigment and the cold protein moiety. Three phenomena may contribute to this time-dependent effect: hot luminescence (86), fluorescence band narrowing, and its red shift on cooling the pigment molecules. It should be noted that if most of the excitations from LHCs will be transferred to RCs already in the course of vibrational relaxation in LHC pigments, the transfer originates from a nonequilibrium or "hot" vibrational state of the donor. A classical Förster transfer takes place from the donor that is in thermal equilibrium with the surrounding thermostat (43). It should be noted also that the hot electronic energy transfer (87) gives the degree of polarization qualitatively similar to reference 20.

The possible interpretation of the experimental results (18, 19) as a consequence of a microscopic solvation dynamics of polar solution (88) is not feasible, because the protein dynamics freeze almost out already at 160 K (22). The local heating considerations do not work here either, because the system is restricted not by the pigment molecule anymore but by the whole surrounding protein (see the discussion in reference 89).

Returning to our initial interpretation of picosecond fluorescence kinetics, let us try to answer the question, what limits the exciton lifetime in PSU: excitation migration or trapping? According to the algorithm proposed in reference 5, we can distinguish these two cases by dividing the zero moment of fluorescence kinetics $\int I(t)\,dt$ into a sum of two constants: the first passage time τ_{FP} and the trapping time τ_T. τ_{FP} is the average time the antenna excitation takes to reach RC special pair P. τ_T is the average time for trapping the excitation that starts from P. $\tau_T \neq \tau_{RC}$ because of a nonabsolute trap, and the excitation may jump several times from P to the antenna and back. If $\tau_{FP} \gg \tau_T$, then the process is migration limited; in the opposite case it is trapping limited. When the model parameters found for the case of active photosynthesis (300 K, RCs open) are used, we get $\tau_{FP} = 2.3\tau_T$. It means that the actual case, according to our model, is somewhere between migration limited and trapping limited.

There seems to be a contradiction between the relatively long hopping time we have in our model and the high annihilation efficiency of excitations in bacteria (for a review see reference 90), which deserves more thorough analysis and will be discussed in more detail elsewhere. We only note that the decrease of the number of connected antenna molecules, between which the energy transfer is possible at lower temperatures revealed in the annihilation experiment (91), is in line with our model and is probably caused by the localization of excitations to the most red molecules within IDF. It should also be noted that the definition of the hopping time depends on the structure of the basic unit between which the hopping takes place. If one compares the hopping time estimated here to the ones obtained from annihilation studies, one has to use the same structural assumptions in both cases.

VI. CONCLUSIONS

The kinetic model of primary energy transfer and trapping in photosynthetic membranes has been developed. A comparison with picosecond time-and-frequency-resolved fluorescence data in a wide temperature range of 4–300 K has proved its reliability at high temperatures. At low temperatures the model fails to reproduce the experimental data accurately enough. The reasons could be the lack of knowledge about the real structure of PSU, inaccurate parameters used, or neglecting the local heating and cooling effects in the model. To catch the latter effects, very accurate measurements on LHCs by using different excitation wavelengths together with model calculations based on reliable structural data about LHCs are needed.

APPENDIX A

According to reference 39, $R_0^6(\nu_{ij}, T_0)$ for homogeneously broadened spectra at relatively high temperature, when their shapes are well Gaussian, can be taken in the following form:

$$R_0^6(\nu_{ij}, T_0) = \frac{C}{2\sqrt{\pi}\sigma_h(T_0)} \exp\left[\frac{-(\nu_{ij} - S)^2}{4\sigma_h(T_0)^2}\right], \quad \text{(A1)}$$

where C is a constant and other parameters are as explained in the text. The properties of the convolution of two Gaussians are used here. Inhomogeneously broadened experimentally observable spectra are the convolutions of the IDF $\rho(\nu)$ and homogeneous spectra (44). Assuming IDF to be Gaussian, instead of $\sigma_h(T)$ we have $\sqrt{\sigma_h(T)^2 + \sigma_{idf}^2}$, which through experimentally determined spectral overlap gives

$$R_{0E}^6 = \frac{C}{2\sqrt{\pi}\sqrt{\sigma_h(T_0)^2 + \sigma_{idf}^2}} \exp\left[\frac{-S^2}{4(\sigma_h(T_0)^2 + \sigma_{idf}^2)}\right]. \quad \text{(A2)}$$

Eqs. A1 and A2 lead to Eq. 7.

When R_{0E}^6 is determined by measuring of the fluorescence depolarization rate, then the quantity actually measured is:

$$R_{0E}^6 = \int\int_{-\infty}^{\infty} \rho(\nu_i)\rho(\nu_j)R_0^6(\nu_{ij}, T_0)\,d\nu_i\,d\nu_j. \quad \text{(A3)}$$

After necessary integrations, one again has Eq. A2.

APPENDIX B

The convolution of two Lorentzians is also a Lorentzian with an added-up FWHM $\Gamma = \Gamma_i + \Gamma_j$. For phonon wings we get

$$Q_i \oplus Q_j(\nu_{ij}) = H_{ij}\left[\frac{2}{m_{ij}^3}(\exp(m_{ij}\nu_j) - \exp(m_{ij}\nu_i)) + \frac{\nu_{ij}}{m_{ij}^2}(\exp(m_{ij}\nu_j) + \exp(m_{ij}\nu_i))\right], \quad \text{(B1)}$$

$$H_{ij} = \frac{\exp\left(\frac{\mu_i\nu_j - \mu_j\nu_i}{\mu_i\mu_j}\right)}{\mu_i\mu_j}, \quad \text{(B2)}$$

$$m_{ij} = \frac{\mu_j - \mu_i}{\mu_i\mu_j}. \quad \text{(B3)}$$

If $\mu_i \to \mu_j = \mu$, then we get

$$Q_i \oplus Q_j(\nu_{ij}) = \frac{\nu_{ij}^3}{6\mu^4}\exp\left(\frac{-\nu_{ij}}{\mu}\right). \quad \text{(B4)}$$

APPENDIX C

Suppose that the angle between the polarization vector of the exciting light $\vec{e}$ and the transition dipole moment of the site j is ξ_j, then the emission intensity from the site j polarized parallel to $\vec{e}$ is $E_j^{\parallel} = \cos^2\xi_j$. For simplicity, the units of dipole moment strength are used here. To get $E_j^{\perp}$, we have to average over all possible emission directions perpendicular to $\vec{e}$: $E_j^{\perp} = \frac{1}{2}\sin^2\xi_j = \frac{1}{2}(1 - E_j^{\parallel})$.

According to Eq. 23, we can write

$$I_j^{\parallel} = \sum_i d_{ji}^{\parallel} G_{ji}, \quad \text{(C1)}$$

$$I_j^{\perp} = \sum_i d_{ji}^{\perp} G_{ji}, \quad \text{(C2)}$$

where

$$d_{ji}^{\parallel} = \langle E_j^{\parallel} A_i \rangle \quad \text{(C3)}$$

$$d_{ji}^{\perp} = \langle E_j^{\perp} A_i \rangle = \tfrac{1}{2}[\langle A_i \rangle - \langle E_j^{\parallel} A_i \rangle]. \quad \text{(C4)}$$

The brackets $\langle\ \rangle$ denote here the average over all possible PSU orientations; the mutual dipole moment orientations inside PSU are unchanged.

After completing all necessary integrations, we get $\langle A_i \rangle = \frac{1}{3}$ and $d_{ji}^{\parallel} = 1/15(1 + 2\cos^2\alpha_{ij})$, where α_{ij} is the angle between the transition dipole moments of the sites i and j. As the orientation-dependent part of $d_{ji}^{\parallel}$ and $d_{ji}^{\perp}$ is determined with the precision of a constant multiplier, we finally get

$$d_{ji}^{\parallel} = 1 + 2\cos^2\alpha_{ij} \quad \text{(C5)}$$

$$d_{ji}^{\perp} = 2.5 - 0.5 d_{ji}^{\parallel}. \quad \text{(C6)}$$

APPENDIX D

Consider the excitation being at the site i. $w_i = \sum_j^N W_{ij}$ is the total rate of the excitation leaving from that site. N is the number of different leaving channels (losses, trapping by RC, transfer to other sites). The moment t_0, when excitation leaves that site, is determined by

$$\int_0^{t_0} \exp(-w_i t)\, dt = x, \quad \text{(D1)}$$

where x is a random number between 0 and $1/w_i$. From Eq. D1 we get

$$t_0 = -\frac{1}{w_i}\ln(1 - w_i x). \quad \text{(D2)}$$

To find the leaving channel j, we divide the segment $[0, w_i]$ into N subsegments with the lengths W_{ij}. By generating a random number between 0 and w_i and finding the subsegment hit by that number, the decay channel is found.

If excitation is transferred to another site, the procedure is repeated. If excitation leaves the system, new excitation is generated randomly, taking into account the absorbance of each site and the procedure is started all over again.

We are indebted to Drs. V. I. Godik, I. Tehver, V. A. Shuvalov, K. Timpmann, G. Trinkūnas, and L. Valkunas for many useful discussions and critical remarks.

Received for publication 2 December 1991 and in final form 12 May 1992.

REFERENCES

1. Zuber, H. 1987. The structure of light-harvesting pigment-protein complexes. *In* The Light Reactions. J. Barber, editor. Elsevier Science Publishing Co. Inc., New York. 197–259.
2. Robinson, G. W. 1967. Excitation transfer and trapping in photosynthesis. *Brookhaven Symp. Biol.* 19:16–48.
3. Pearlstein, R. M. 1967. Migration and trapping of excitation quanta in photosynthetic unit. *Brookhaven Symp. Biol.* 19:8–14.
4. Barber, J. 1978. Biophysics of photosynthesis. *Rep. Prog. Phys.* 41:1157–1199.
5. Pearlstein, R. M. 1982. Exciton migration and trapping in photosynthesis. *Photochem. Photobiol.* 35:835–844.
6. Shipman, L. L. 1980. Excitation migration in photosynthetic systems on the picosecond timescale. *Photochem. Photobiol.* 31:157–167.
7. Kudzmauskas, S., L. Valkunas, and A. Yu. Borisov. 1983. A theory of excitation transfer in photosynthetic units. *J. Theor. Biol.* 105:13–23.
8. Skala, L., and P. Jungwirth. 1989. Theory of excitation energy transfer in the primary processes of photosynthesis. II. Group symmetry analysis of the bacterial light-harvesting complex. *Chem. Phys.* 137:93–98.
9. Källebring, B., and Ö. Hansson. 1991. A theoretical study of the effect of charge recombination on the transfer and trapping of excitation energy in photosynthesis. *Chem. Phys.* 149:361–372.
10. Borisov, A. Yu., A. M. Freiberg, V. I. Godik, K. K. Rebane, and K. E. Timpmann. 1985. Kinetics of picosecond bacteriochlorophyll luminescence in vivo as a function of the reaction center state. *Biochim. Biophys. Acta.* 807:221–229.
11. Duysens, L. N. M. 1986. Introduction to (bacterio)chlorophyll emission: a historical perspective. *In* Light Emission by Plants and Bacteria. Govindjee, J. Amesz, and D. C. Fork, editors. Academic Press, Inc., Orlando, FL. 3–28.
12. Litvin, F. F., and V. A. Sineshchenkov. 1975. Molecular organization of chlorophyll and energetics of the initial stages in photosynthesis. *In* Bioenergetics of Photosynthesis. Govindjee, editor. Academic Press, New York. 619–661.

13. Fetisova, Z. G., A. Yu. Borisov, and M. V. Fok. 1985. Analysis of structure-function correlations in light-harvesting photosynthetic antenna: structure optimization parameters. *J. Theor. Biol.* 112:41–75.

14. Seely, G. R. 1973. Effects of spectral variety and molecular orientation on energy trapping in the photosynthetic unit: a model calculation. *J. Theor. Biol.* 40:173–187.

15. Monger, T. G., and W. W. Parson. 1977. Singlet-triplet fusion in *Rhodopseudomonas sphaeroides* chromatofores. A probe of the organization of the photosynthetic apparatus. *Biochim. Biophys. Acta.* 460:393–407.

16. Sundström, V., R. van Grondelle, H. Bergström, E. Åkesson, and T. Gillbro. 1986. Excitation energy transport in the bacteriochlorophyll antenna systems of *Rhodospirillum rubrum* and *Rhodobacter sphaeroides* studied by low-intensity picosecond spectroscopy. *Biochim. Biophys. Acta.* 851:431–446.

17. Freiberg, A., V. I. Godik, T. Pullerits, and K. Timpmann. 1989. Picosecond dynamics of directed excitation transfer in spectrally heterogeneous light-harvesting antenna in purple bacteria. *Biochim. Biophys. Acta.* 973:93–104.

18. Freiberg, A., V. I. Godik, and K. Timpmann. 1987. Spectral dependence of the fluorescence lifetime of *Rhodospirillum rubrum.* Evidence for inhomogeneity of B880 absorption band. *In* Progress in Photosynthesis Research. Vol. 1. J. Biggins, editor. Martinus Nijhoff, Dordrecht, The Netherlands: 45–48.

19. Timpmann, K., A. Freiberg, and V. I. Godik. 1991. Picosecond kinetics of light excitations in photosynthetic purple bacteria in the temperature range of 300–4 K. *Chem. Phys. Lett.* 182:617–622.

20. Kramer, H.-J., J. D. Pennoyer, R. van Grondelle, W. H. J. Westerhuis, R. A. Niederman, and J. Amesz. 1984. Low temperature optical properties and pigment organization of the B875 light-harvesting bacteriochlorophyll protein complex of purple photosynthetic bacteria. *Biochim. Biophys. Acta.* 767:335–344.

21. Avarmaa, R. A., and K. K. Rebane. 1985. High-resolution optical spectra of chlorophyll molecules. *Spectrochim. Acta Part A Mol. Spectrosc.* 41:1365–1380.

22. Ormos, P., A. Ansari, D. Braunstein, B. R. Cowen, H. Frauenfelder, M. K. Hong, I. E. T. Iben, T. B. Sauke, P. J. Steinbach, and R. D. Young. 1990. Inhomogeneous broadening in spectral bands of carbonmonoxymyoglobin. The connection between spectral and functional heterogeneity. *Biophys. J.* 57:191–199.

23. Lee, I.-J., J. K. Gillie, and C. K. Johnson. 1989. Photochemical hole burning in bacteriorhodopsin. *Chem. Phys. Lett.* 156:227–232.

24. Köhler, W., J. Friedrich, R. Fischer, and H. Scheer. 1988. High resolution frequency selective photochemistry of phycobilisomes at cryogenic temperatures. *J. Chem. Phys.* 89:871–874.

25. Johnson, S. G., and G. J. Small. 1991. Excited-state structure and energy-transfer dynamics of the bacteriochlorophyll *a* antenna complex from *Prosthecochloris aestuarii. J. Phys. Chem.* 95:471–479.

26. Van der Laan, H., Th. Schmidt, R. W. Visschers, K. J. Visscher, R. van Grondelle, and S. Völker. 1990. Energy transfer in the B800–850 antenna complex of purple bacteria *Rhodobacter sphaeroides:* a study by spectral hole-burning. *Chem. Phys. Lett.* 170:231–238.

27. Gillie, J. K., G. J. Small, and J. H. Golbeck. 1989. Nonphotochemical hole burning of the native antenna complex of photosystem I (PSI-200). *J. Phys. Chem.* 93:1620–1627.

28. Meech, S. R., A. J. Hoff, and D. A. Wiersma. 1985. Evidence for a very early intermediate in bacterial photosynthesis. A photon-echo and hole-burning study of the primary donor band in *Rhodopseudomonas sphaeroides. Chem. Phys. Lett.* 121:287–292.

29. Vink, K. J., S. De Boer, J. J. Plijter, A. J. Hoff, and D. A. Wiersma. 1987. Optical dynamics of the reaction center of photosystem II. A hole-burning and photon-echo study. *Chem. Phys. Lett.* 142:433–438.

30. Mauring, K., I. Renge, and R. Avarmaa. 1987. A spectral hole-burning study of long-wavelength chlorophyll *a* forms in greening leaves at 5 K. *FEBS (Fed. Eur. Biochem. Soc.) Lett.* 223:165–168.

31. Kirmaier, C., and D. Holten. 1990. Evidence that a distribution of bacterial reaction centers underlies the temperature and detection-wavelength dependence of the rates of the primary electron-transfer reactions. *Proc. Natl. Acad. Sci. USA.* 87:3552–3556.

32. Bodunov, E. N., and V. A. Malyshev. 1984. Kinetics of the luminescence of inhomogeneously broadened systems at low temperature. *J. Appl. Spectrosc. (USA).* 41:1123–1126.

33. Lyo, S. K., T. Holstein, and R. Orbach. 1978. Spectral and spatial diffusion in a disordered system. *Phys. Rev. B.* 18:1637–1640.

34. Parson, R. P., and R. Kopelmann. 1985. A self-consistent theory of nonequilibrium excitation transport in energetically disordered systems. *J. Chem. Phys.* 82:3692–3704.

35. Movaghar, B., M. Grünewald, B. Ries, H. Bässler, and D. Würtz. 1986. Diffusion and relaxation of energy in disordered organic and inorganic materials. *Phys. Rev. B.* 33:5545–5554.

36. Huber, D. L., and W. Y. Ching. 1990. Time-domain analysis of the dynamics of Frenkel excitons in disordered systems. *Phys. Rev. B.* 42:7718–7724.

37. Jean, J. M., C.-K. Chan, G. R. Fleming, and T. G. Owens. 1989. Excitation transport and trapping on spectrally disordered lattices. *Biophys. J.* 56:1203–1215.

38. Freiberg, A., V. I. Godik, T. Pullerits, and K. Timpmann. 1990. *In* Current Research in Photosynthesis. Vol. 2. M. Baltscheffski, editor. Kluwer, Amsterdam. 157–160.

39. Pullerits, T., and A. Freiberg. 1991. Picosecond fluorescence of simple photosynthetic membranes: evidence of spectral inhomogeneity and directed energy transfer. *Chem. Phys.* 149:409–418.

40. Freiberg, A., and T. Pullerits. 1990. Energy transfer and trapping in spectrally disordered photosynthetic membranes. *In* Reaction Centres of Photosynthetic Bacteria. M.-E. Michel-Beyerle, editor. Springer-Verlag, Berlin. 339–348.

41. Hunter, C. N., R. van Grondelle, and J. D. Olsen. 1989. Photosynthetic antenna proteins: 100 ps before photochemistry starts. *Trends Biochem. Sci.* 14:72–76.

42. Kaplan, S., and C. J. Arntzen. 1982. Photosynthesis. Vol. 1. Energy Conversion by Plants and Bacteria. Govindjee, editor. Academic Press, New York.

43. Agranovich, V. M., and M. D. Galanin. 1982. Electronic excitation energy transfer in condensed matter. North-Holland, Amsterdam.

44. Rebane, K. K. 1970. Impurity Spectra of Solids. Plenum Press, New York.

45. Osad'ko, I. S. 1979. Determination of electron-phonon coupling from structured optical spectra of impurity centers. *Sov. Phys. Usp.* 22:311–329.

46. Avarmaa, R., R. Jaaniso, K. Mauring, I. Renge, and R. Tamkivi. 1986. Influence of energy transfer on the structure of site-selection spectra of molecules. *Mol. Physics.* 57:605–621.

47. Goedheer, J. C. 1972. Temperature dependence of absorption and fluorescence spectra of bacteriochlorophylls *in vivo* and *in vitro. Biochem. Biophys. Acta.* 275:169–176.

48. Goedheer, J. C. 1973. Fluorescence polarization and pigment ori-

entation in photosynthetic bacteria. *Biochim. Biophys. Acta.* 292:665–676.

49. Woodbury, N. W. T., and W. W. Parson. 1984. Nanosecond fluorescence from isolated photosynthetic reaction centers of *Rhodopseudomonas sphaeroides. Biochim. Biophys. Acta.* 767:345–361.
50. Schenck, C. C., W. W. Parson, D. Holten, M. Windsor, and A. Sarai. 1981. Temperature dependence of electron transfer between bacteriopheophytin and ubiquinone in protonated and deuterated reaction centers of *Rhodopseudomonas sphaeroides. Biophys. J.* 36:479–489.
51. Fleming, G. R., J. R. Martin, and J. Breton. 1988. Rates of primary electron transfer in photosynthetic reaction centers and their mechanistic implications. *Nature (Lond.).* 333:190–192.
52. Freiberg, A. M., V. I. Godik, S. G. Kharchenko, K. E. Timpmann, A. Yu. Borisov, and K. K. Rebane. 1985. Picosecond fluorescence of reaction centres from *Rhodospirillum rubrum. FEBS (Fed. Eur. Biochem. Soc.) Lett.* 189:341–344.
53. Takiff, L., and S. G. Boxer. 1988. Phosphorescence from the primary electron donor in *Rhodobacter sphaeroides* and *Rhodopseudomonas viridis* reaction centers. *Biochim. Biophys. Acta.* 932:325–334.
54. Mar, T., and G. Gingras. 1984. Photoselection studies of the P-800 band in the photoreaction center of *Rhodospirillum rubrum. Biochim. Biophys. Acta.* 765:125–132.
55. Johnson, S. G., D. Tang, R. Jankowiak, J. M. Hayes, G. J. Small, and D. M. Tiede. 1989. Structure and marker mode of the primary electron donor state absorption of photosynthetic bacteria: hole-burned spectra. *J. Phys. Chem.* 93:5953–5957.
56. Boxer, S. G., R. A. Goldstein, D. J. Lockhart, T. R. Middendorf, and L. Takiff. 1989. Excited states, electron-transfer reactions, and intermediates in bacterial photosynthetic reaction centers. *J. Phys. Chem.* 93:8280–8294.
57. Trissl, H.-W., J. Breton, J. Deprez, A. Dobek, and W. Leibl. 1990. Trapping kinetics, annihilation, and quantum yield in the photosynthetic purple bacterium *Rps. viridis* as revealed by electric measurement of the primary charge separation. *Biochim. Biophys. Acta.* 1015:322–333.
58. Friesner, R. A., and Y. Won. 1989. Spectroscopy and electron transfer dynamics of the bacterial photosynthetic reaction center. *Biochim. Biophys. Acta.* 977:99–122.
59. Grad, J., G. Hernandez, and S. Mukamel. 1988. Radiative decay and energy transfer in molecular aggregates: the role of intermolecular dephasing. *Phys. Rev. A.* 37:3835–3846.
60. De Boer, S., and Wiersma, D. A. 1990. Dephasing-induced damping of superradiant emission in J-aggregates. *Chem. Phys. Lett.* 165:45–53.
61. Scherz, A., and W. W. Parson. 1984. Oligomers of bacteriochlorophyll and bacteriopheophytin with spectroscopic properties resembling those found in photosynthetic bacteria. *Biochim. Biophys. Acta.* 766:653–665.
62. Fetisova, Z. G., L. V. Shibaeva, and M. V. Fok. 1989. Biological expedience of oligomerization of chlorophyllous pigments in natural photosynthetic systems. *J. Theor. Biol.* 140:167–184.
63. Gingras, G., and R. Picorel. 1990. Supramolecular arrangement of *Rhodospirillum rubrum* B880 holochrome as studied by radiation inactivation and electron paramagnetic resonance. *Proc. Natl. Acad. Sci. USA.* 87:3405–3409.
64. Chang, M. C., P. M. Callahan, P. S. Parkes-Loach, T. M. Cotton, and P. A. Loach. 1990. Spectroscopic characterization of the light-harvesting complex of *Rhodospirillum rubrum* and its structural subunit. *Biochemistry.* 29:421–429.
65. Ghosh, R., and R. Bachofen. 1989. Die molekulare Struktur der photosynthetischen Membranen bei anoxygenen phototropen Bakterien. *Forum Mikrobiologie.* 12:556–564.
66. Miller, K. R. 1982. Three-dimensional structure of a photosynthetic membrane. *Nature (Lond.).* 300:53–55.
67. Welte, W., and W. Kreutz. 1982. Formation, structure and composition of a planar hexagonal lattice composed of specific protein-lipid complexes in the thylakoid membranes of *Rhodopseudomonas viridis. Biochim. Biophys. Acta.* 692:479–488.
68. Miller, J. F., S. B. Hinchigeri, P. S. Parkes-Loach, P. M. Callahan, J. R. Sprinkle, J. R. Riccobono, and P. A. Loach. 1987. Isolation and characterization of a subunit form of the light-harvesting complex of *Rhodospirillum rubrum. Biochemistry.* 26:5055–5062.
69. Van Mourik, F., J. R. Oord, K. J. Visscher, P. S. Parkes-Loach, P. A. Loach, R. W. Visschers, and R. van Grondelle. 1991. Exciton interactions in the light-harvesting antenna of photosynthetic bacteria studied with triplet-singlet spectroscopy and singlet-triplet annihilation. *Biochim. Biophys. Acta.* 1059:111–119.
70. Freiberg, A., T. Pullerits, and K. Timpmann. 1990. Time-resolved fluorescence spectroscopy of photosynthetic membranes. Experiment and model simulations. *In* Time-Resolved Laser Spectroscopy in Biochemistry II. SPIE Vol. 1204. 727–735.
71. Breton, J. 1985. Orientation of the chromophores in the reaction center of *Rhodopseudomonas viridis.* Comparison of low-temperature linear dichroism spectra with a model derived from X-ray crystallography. *Biochim. Biophys. Acta.* 810:235–245.
72. Breton, J., D. L. Farkas, and W. W. Parson. 1985. Organization of the antenna bacteriochlorophylls around the reaction center of *Rhodopseudomonas viridis* investigated by photoselection techniques. *Biochim. Biophys. Acta.* 808:421–427.
73. Schatz, G., and A. R. Holzwarth. 1986. Mechanisms of chlorophyll fluorescence revisited: prompt or delayed emission from photosystem II with closed reaction centers? *Photosynth. Res.* 10:309–318.
74. Tronrud, D. E., M. F. Schmid, and B. W. Matthews. 1986. Structure and X-ray amino acid sequence of a bacteriochlorophyll *a* protein from *Prostecochloris aestuarii* refined at 1.9 Å resolution. *J. Mol. Biol.* 188:443–454.
75. Holzwarth, A., E. Bittersmann, W. Reuter, and W. Wehrmeyer. 1990. Studies on chromophore coupling in isolated phycobiliproteins III. Picosecond excited state kinetics and time-resolved fluorescence spectra of different allophycocyanins from *Mastigocladus laminosus. Biophys. J.* 57:133–145.
76. Kenkre, V. M., and D. Schmid. 1985. Coherence in singlet-exciton motion in anthracene crystals. *Phys. Rev. B.* 31:2430–2436.
77. Kenkre, V. M., and R. S. Knox. 1974. Generalized-master-equation theory of excitation transfer. *Phys. Rev. B.* 9:5279–5290.
78. Razjivin, A. P., R. V. Danielius, R. A. Gadonas, A. Yu. Borisov, and A. S. Piskarskas. 1982. The study of excitation transfer between light-harvesting antenna and reaction center in chromatophores from purple bacterium *Rhodospirillum rubrum* by selective picosecond spectroscopy. *FEBS (Fed. Eur. Biochem. Soc.) Lett.* 143:40–44.
79. Ritt-Fischer, M. R. 1991. Studies on the primary processes in bacterial photosynthesis. Ph.D. thesis. Leiden, The Netherlands. 130 pp.
80. James, D. R., and W. R. Ware. 1985. A fallacy in the interpretation of fluorescence decay parameters. *Chem. Phys. Lett.* 120:455–459.
81. Dlott, D. D. 1990. Vibrational cooling (and heating) of large molecules in solids. *J. Lumin.* 45:397–400.
82. Seilmeier, A., and W. Kaiser. 1988. Ultrashort intramolecular and intermolecular vibrational energy transfer of polyatomic mole-

cules in liquids. *In* Ultrashort Laser Pulses and Applications. W. Kaiser, editor. Springer-Verlag, Berlin. 279–317.

83. Petrich, J. W., J. L. Martin, D. Houde, C. Poyart, and A. Orszag. 1987. Time-resolved Raman spectroscopy with subpicosecond resolution: vibrational cooling and delocalization of strain energy in photodissociated (carbonmonoxy) hemoglobin. *Biochemistry.* 26:7914–7923.
84. Henry, E. R., W. A. Eaton, and R. M. Hochstrasser. 1986. Molecular dynamics simulations of cooling in laser-excited heme proteins. *Proc. Natl. Acad. Sci. USA.* 83:8982–8986.
85. Rodriguez, J., C. Kirmaier, and D. Holten. 1991. Time-resolved and static optical properties of vibrationally excited porphyrins. *J. Chem. Phys.* 94:6020–6029.
86. Rebane, K., and P. Saari. 1978. Hot luminescence and relaxation processes in resonant secondary emission of solid matter. *J. Lumin.* 16:223–243.
87. Tehver, I. Y., and V. V. Hizhnyakov. 1976. Radiationless transfer of electronic excitation during vibrational relaxation. *Sov. Phys.-JETP.* 42:305–310.
88. Nagarajan, V., A. M. Brearley, T.-J. Kang, and P. F. Barbara. 1987. Time-resolved spectroscopic measurements on microscopic solvation dynamics. *J. Chem. Phys.* 86:3183–3196.
89. Valkunas, L., V. Liuolia, and A. Freiberg. 1991. Picosecond processes in chromatophores at various light intensities. *Photosynth. Res.* 27:83–95.
90. Van Grondelle, R. 1985. Excitation energy transfer, trapping and annihilation in photosynthetic systems. *Biochim. Biophys. Acta.* 811:147–195.
91. Vos, M., R. van Grondelle, F. W. van der Kooij, D. van de Poll, J. Amesz, and L. N. M. Duysens. 1986. Singlet-singlet annihilation at low temperatures in the antenna of purple bacteria. *Biochim. Biophys. Acta.* 850:501–512.